

Crystal growth, spectroscopy and first laser operation of a novel disordered tetragonal Tm:Na₂La₄(WO₄)₇ tungstate crystal

Lizhen Zhang^a, Shijia Sun^a, Zhoubin Lin^a, Haifeng Lin^a, Ge Zhang^a, Xavier Mateos^b, Josep Maria Serres^b, Magdalena Aguiló^b, Francesc Díaz^b, Pavel Loiko^c, Yicheng Wang^d, Uwe Griebner^d, Valentin Petrov^d, Elena Vilejshikova^e and Weidong Chen^{a,d,*}

^aKey Laboratory of Optoelectronic Materials Chemistry and Physics, Fujian Institute of Research on the Structure of Matter, Chinese Academy of Sciences, Fuzhou, 350002 Fujian, China

^bUniversitat Rovira i Virgili, Departament Química Física i Inorgànica, Física i Cristal·lografia de Materials i Nanomaterials (FiCMA-FiCNA)-EMaS, Campus Sescelades, E-43007, Tarragona, Spain

^cITMO University, 49 Kronverkskiy Pr., 197101 St. Petersburg, Russia

^dMax Born Institute for Nonlinear Optics and Short Pulse Spectroscopy, 2A Max-Born-Str., D-12489 Berlin, Germany

^eCenter for Optical Materials and Technologies, BNTU, 65/17 Nezavisimosti Ave., 220013 Minsk, Belarus

*Corresponding author, e-mail: chenweidong@fjirsm.ac.cn

Abstract Tm³⁺:Na₂La₄(WO₄)₇, a disordered tetragonal scheelite-type tungstate crystal, is grown by the Czochralski method. The polarized absorption, stimulated-emission and gain cross-section spectra are determined. The maximum σ_{SE} is 1.62×10^{-20} cm² at 1788.6 nm for σ -polarization. The Judd-Ofelt parameters for Tm³⁺ are $\Omega_2 = 10.321$, $\Omega_4 = 0.183$ and $\Omega_6 = 2.122$ [10^{-20} cm²]. The radiative lifetime of the ³F₄ state is 1.63 ms. Raman spectroscopy reveals a maximum phonon energy of 923 cm⁻¹. Laser operation under diode-pumping is achieved with both *a*-cut and *c*-cut Tm:Na₂La₄(WO₄)₇ crystals, reaching a maximum output power for the *a*-cut of 715 mW at ~1937 nm with a slope efficiency of 34%. Microchip laser operation using the *c*-cut crystal yields a slope efficiency of 41%. The Tm:Na₂La₄(WO₄)₇ crystal is promising for mode-locked lasers due to its broadband emission.

Keywords: seven tungstates; thulium ions; absorption; luminescence; Judd-Ofelt theory; laser operation.

1. Introduction

The Thulium (Tm^{3+}) ion (electronic configuration: $[\text{Xe}]4f^{12}$) plays an important role in laser physics due to its broadband eye-safe emission at $\sim 2 \mu\text{m}$ related to the ${}^3\text{F}_4 \rightarrow {}^3\text{H}_6$ 4f-4f transition. Tm lasers are used in medicine, remote sensing (LIDAR) and spectroscopy. One of the most studied hosts for Tm^{3+} doping are the scheelite (CaWO_4) type (space group $I\bar{4}$) tetragonal (i.e. uniaxial) sodium double tungstate crystals, $\text{NaT}(\text{WO}_4)_2$, where $\text{T} = \text{Gd}, \text{Y}, \text{Lu}$ or La [1]. In the $\text{NaT}(\text{WO}_4)_2$ lattice, the $2b$ and $2d$ sites (both possessing the same S_4 symmetry) are statistically occupied by the univalent Na^+ and trivalent T^{3+} cations. The laser-active rare-earth ions, e.g., Tm^{3+} , will replace the T^{3+} cations in both sites [2]. The local disorder of the Tm^{3+} -doped $\text{NaT}(\text{WO}_4)_2$ crystals is then explained by the short-range $\text{Na}^+/\text{T}^{3+}$ distribution, i.e., the second shell of cations around each $2b$ or $2d$ sites [1]. Due to the local disorder, Tm^{3+} -doped $\text{NaT}(\text{WO}_4)_2$ crystals feature broad absorption and emission spectral bands for polarized light [1-4]. The upper laser level (${}^3\text{F}_4$) lifetime of Tm^{3+} is relatively long and amounts to $\sim 1 \text{ ms}$ [1].

The suitable spectroscopic properties of the $\text{Tm}:\text{NaT}(\text{WO}_4)_2$ crystals enabled an efficient pumping at $\sim 0.8 \mu\text{m}$ (the ${}^3\text{H}_6 \rightarrow {}^3\text{H}_4$ transition of Tm^{3+}) by AlGaAs laser diodes or Ti:Sapphire lasers [1,2,5], linearly polarized laser output and broad wavelength tuning of the laser emission in the continuous-wave (CW) regime [5]. An *a*-cut $\text{Tm}:\text{NaLu}(\text{WO}_4)_2$ laser generated 0.49 W of σ -polarized output at 1924 nm with a slope efficiency η of 48.5% (with respect to the absorbed pump power) when pumped by a Ti:Sapphire laser at 800 nm [2]. In [1], an *a*-cut $\text{Tm}:\text{NaY}(\text{WO}_4)_2$ laser was continuously tuned from 1847 to 2069 nm (for σ -polarization).

In the present work, we report on the development of a novel disordered scheelite-type tungstate laser crystal, $\text{Tm}:\text{Na}_2\text{La}_4(\text{WO}_4)_7$. Its ideal chemical formula can be represented as $\text{Na}_x\text{La}_y(\text{WO}_4)_2$ where $x = 4/7$ and $y = 8/7$, so that the charge compensation is maintained. Recently, lasing of $\text{Na}_2\text{La}_4(\text{WO}_4)_7$ doped with Nd^{3+} was demonstrated [6], however, the output power was only 80 mW at 1060 nm with $\eta = 7\%$ under quasi-CW pumping. An isostructural $\text{Na}_2\text{La}_4(\text{MoO}_4)_7$ crystal is also known [7]. The search for novel crystals within the family of the tetragonal tungstates is motivated by the inferior thermal and thermo-optical properties of the conventional $\text{NaT}(\text{WO}_4)_2$ crystals, namely, low thermal conductivity ($\sim 1 \text{ W/mK}$) and negative thermo-optic coefficients, dn/dT [8], limiting the power scaling capabilities of these crystals as compared to the monoclinic (space group $C2/c$) double tungstates, e.g., $\text{Tm}:\text{KLu}(\text{WO}_4)_2$ [9] or tungstates, e.g., $\text{Tm}:\text{MgWO}_4$ [10].

2. Crystal growth and structure

The $\text{Na}_2\text{La}_4(\text{WO}_4)_7$ crystal melts congruently at 1252 °C [6]. As a consequence, it can be grown by the Czochralski method. The raw materials for the growth charge were synthesized by a solid-state reaction, $\text{Na}_2\text{CO}_3 + (2-2x)\text{La}_2\text{O}_3 + 2x\text{Tm}_2\text{O}_3 + 7\text{WO}_3 \rightarrow \text{Na}_2(\text{La}_{1-x}\text{Tm}_x)_4(\text{WO}_4)_7 + \text{CO}_2\uparrow$. The chemicals used for crystal growth were Na_2CO_3 and WO_3 (analytical grade purity), as well as La_2O_3 and Tm_2O_3 (99.99% purity). Stoichiometric amounts of raw materials were weighed, mixed, ground and extruded to form the pellets. Then, such pellets were placed in an alumina crucible and kept at 950 °C for 48 h. This process was re-

peated two times to ensure pure polycrystalline materials. The synthesized raw materials were placed in a platinum crucible located in a 2 kHz furnace and heated slightly above the melting point for 1 h. Then, the temperature was decreased to the crystallization point. The crystal was grown at a pulling rate of 1–1.5 mm/h and a rotation rate of 10–15 rpm along the [100] crystallographic direction. The grown crystal was cooled down to room temperature at a cooling rate of 15–20 °C/h.

A Tm:Na₂La₄(WO₄)₇ crystal with dimensions of Ø20×35 mm³ was grown within four days, see Fig. 1(a). It was crack-free and transparent but had a slight green coloration. We attributed this slight green coloration of the sample to the impurities or defects in the crystal with a strong absorption in the region of 350–696 nm, which might introduce some detrimental effects to the laser operation of this material. The Tm³⁺-ion concentration in the grown crystal, $N_{\text{Tm}} = 1.43 \times 10^{20}$ at/cm³ (1.36 at.%) was measured by inductively coupled plasma atomic emission spectrometry. Since the ion distribution shows a certain concentration gradient in the crystal during the crystal growth process, we have measured the averaged concentration. We used the average concentration of Tm³⁺ ion in Na₂La₄(WO₄)₇ to calculate the segregation coefficient. The calculated segregation coefficient of the Tm³⁺ is $K_{\text{Tm}}=0.38$.

The structure and the phase purity of the grown crystal were confirmed by X-ray powder diffraction (XRD), Fig. 1(b). The structure was refined with the Rietveld method. Tm:Na₂La₄(WO₄)₇ is tetragonal (defect scheelite-type structure with space group $I4-S_4^2$, No. 82) and optically uniaxial (optical axis is parallel to the *c*-axis). It possesses two crystallographic sites (2*b* and 2*d*) statistically occupied by the La³⁺/Tm³⁺ and Na⁺ cations following the atomic ratio La/Tm:Na = 2:1 (in total). For both sites, the La³⁺ cations are VIII-fold O²⁻ coordinated (ionic radius: 1.16 Å), Fig. 2. The ionic radius of Tm³⁺ (0.994 Å) is smaller than that of La³⁺ and thus an additional effect on the crystal field strength is expected.

The determined lattice parameters of Tm:Na₂La₄(WO₄)₇ are $a = b = 5.35526(7)$ Å, $c = 11.68568(2)$ Å, the volume of the unit-cell $V = 335.132(8)$ Å³, and the calculated density $\rho_{\text{calc}} = 4.901$ g/cm³. The reduced chi-squared $\chi^2 = (R_{\text{wp}}/R_{\text{exp}})^2$ was 1.387. The determined lattice constants are close to those of NaLa(WO₄)₂, $a = 5.3575(7)$ Å, $c = 11.671(2)$ Å [1], and of 0.41 at.% Nd:Na₂La₄(WO₄)₇, $a = 5.355$ Å, $c = 11.68$ Å [6].

3. Spectroscopic characterization

For the spectroscopic studies, a 3.1 mm-thick rectangular sample was cut along the *a*-axis with an aperture of 3.0(*c*)× 3.0(*a*) mm² giving access to both principal light polarizations, π ($\mathbf{E} \parallel \mathbf{c}$) and σ ($\mathbf{E} \perp \mathbf{c}$). All studies were performed at room temperature (293 K).

3.1. Optical absorption

The absorption spectra of Tm:Na₂La₄(WO₄)₇ corresponding to the transitions from the ³H₆ ground-state to the ³F₄, ³H₅, ³H₄, ³F_{2,3}, ¹G₄ and ¹D₂ excited-states of Tm³⁺ are shown in Fig. 3 for π - and σ -polarizations. The absorption cross-sections were calculated as $\sigma_{\text{abs}} = \alpha_{\text{abs}}/N_{\text{Tm}}$. For the ³H₆ → ³H₄ Tm³⁺ transition suitable for pumping with AlGaAs laser diodes, Fig. 3(d), the maximum σ_{abs} is 4.86×10^{-20} cm² at 794.5 nm for σ -polarization. The full width at half maximum (FWHM) of the absorption band is 5.3 nm. The peak σ_{abs} is much lower for

π -polarization, namely $1.37 \times 10^{-20} \text{ cm}^2$ at 793.6 nm. The polarization anisotropy is less pronounced for the ${}^3\text{H}_6 \rightarrow {}^3\text{F}_4$ transition, Fig. 3(f). This transition can be used for resonant pumping of Tm lasers, e.g., by Raman-shifted Er fiber lasers. The maximum σ_{abs} is $1.33 \times 10^{-20} \text{ cm}^2$ at 1699 nm for π -polarization and $1.24 \times 10^{-20} \text{ cm}^2$ at 1743 nm for σ -polarization. The measured UV absorption edge λ_g for Tm:Na₂La₄(WO₄)₇ is 330 nm (π) and 334 nm (σ) corresponding to a bandgap E_g of $\sim 3.76 \text{ eV}$.

The transition probabilities for the Tm³⁺ ion in Na₂La₄(WO₄)₇ were determined within the standard Judd-Ofelt (J-O) theory [11,12]. All quantities were considered as polarization-averaged, e.g., the experimental absorption oscillator strengths $\langle f_{\text{exp}}^{\Sigma} \rangle = (2f_{\text{exp}}^{\Sigma}(\sigma) + f_{\text{exp}}^{\Sigma}(\pi))/3$ which were determined from the measured absorption spectra, Fig. 3. By applying the J-O theory, we calculated the absorption oscillator strengths for the Tm³⁺ ion $\langle f_{\text{calc}}^{\Sigma} \rangle$, see Table 1. The root mean square (rms) deviation between $\langle f_{\text{exp}}^{\Sigma} \rangle$ and $\langle f_{\text{calc}}^{\Sigma} \rangle$ was 0.566. More details and in particular the squared reduced matrix elements $U^{(k)}$ and the magnetic-dipole (MD) contributions $\langle f_{\text{calc}}^{\text{MD}} \rangle$ can be found in [10,13]. The refractive indices were for Tm:NaLa(WO₄)₂ and taken from [8]. The determined intensity (J-O) parameters are $\Omega_2 = 10.321$, $\Omega_4 = 0.183$ and $\Omega_6 = 2.122 [10^{-20} \text{ cm}^2]$.

3.2. Optical emission

Using the J-O parameters, we calculated the probability of spontaneous transitions $A_{JJ'}$, the luminescence branching ratios $B_{JJ'}$ and the radiative lifetimes, τ_{rad} , of the excited-states of the Tm³⁺ ion. For the squared reduced matrix elements $U^{(k)}$ for emission and the MD contributions $A_{JJ'}^{\text{MD}}$, refer to [10,13]. The results are presented in Table 2. For the upper laser level, ${}^3\text{F}_4$, τ_{rad} is 1.63 ms. For the pump level, ${}^3\text{H}_4$, $\tau_{\text{rad}} = 0.22 \text{ ms}$.

The unpolarized near-IR emission spectrum of Tm:Na₂La₄(WO₄)₇ under excitation at 802 nm (to the ${}^3\text{H}_4$ state) is shown in Fig. 4(a). It contains the emission at 1.4-1.55 μm due to the ${}^3\text{H}_4 \rightarrow {}^3\text{F}_4$ transition and the broad and intense emission at 1.65-2.05 μm due to the ${}^3\text{F}_4 \rightarrow {}^3\text{H}_6$ transition. To calculate the polarized stimulated-emission (SE) cross-sections, σ_{SE} , for this transition, we used the modified reciprocity method [14]. The results are shown in Fig. 4(b). For σ -polarization, the maximum σ_{SE} is $1.62 \times 10^{-20} \text{ cm}^2$ at 1788.6 nm. For π -polarization, the maximum σ_{SE} is slightly lower, $1.44 \times 10^{-20} \text{ cm}^2$ at 1839 nm.

The measured luminescence decay curve (emission at 1800 nm, from the ${}^3\text{F}_4$ state) for the Tm:Na₂La₄(WO₄)₇ crystal is shown in Fig. 4(c). The characteristic decay time τ_{lum} is 1.7 ms which is close to the radiative one (1.63 ms).

The Tm³⁺ ion represents a quasi-three-level laser scheme, therefore, we calculated the gain cross-sections, $\sigma_g = \beta\sigma_{\text{SE}} - (1-\beta)\sigma_{\text{abs}}$, where $\beta = N({}^3\text{F}_4)/N_{\text{Tm}}$ is the inversion ratio, see Fig. 5. Higher cross-sections are obtained for the π -polarization. The gain bandwidth (FWHM) calculated for $\beta = 0.3$ is 110 nm (π) and 108 nm (σ).

3.3. Raman spectroscopy

The vibrational properties of Tm:Na₂La₄(WO₄)₇ were characterized with Raman spectroscopy using polarized light, Fig. 6. Porto's notation $m(nk)\bar{l}$ means the following: m and l stand for the direction of propagation of the excitation and scattered light, respectively, and n

and k – for their polarizations, respectively. Both a -cut and c -cut crystals were studied. The excitation wavelength was 514 nm (Ar⁺ ion laser).

For the NaT(WO₄)₂-type tetragonal crystals, according to the group theory, the irreducible representations at the center of the Brillouin zone ($k = 0$) are: $\Gamma = 3A_g + 5B_g + 5E_g + 5A_u + 3B_u + 5E_u$ of which 13 (A_g , B_g and doubly-degenerated E_g) are Raman-active and the rest are IR-active [15]. For scheelite-type crystals featuring isolated [WO₄] tetrahedra, see Fig. 2, there is an energy gap in the Raman spectra in the 450-700 cm⁻¹ range. This effect is also clearly observed for Tm:Na₂La₄(WO₄)₇. Physically, the bands at such frequencies are related to the double oxygen bridge vibrations (WOOW) and they are observed for monoclinic KLu(WO₄)₂ and MgWO₄ featuring interconnected [WO₆] polyhedra [9,10]. For Tm:Na₂La₄(WO₄)₇, the bands at 758-923 cm⁻¹ are due to the symmetric and asymmetric stretching vibrations (ν) of the [WO₄] groups, the bands at 325-417 cm⁻¹ are due to the [WO₄] bending modes (δ) and the bands at shorter frequencies are due to the external lattice vibrations (L, T). The strongest band contains several peaks at 914 and 923 cm⁻¹. The Raman activity of Na₂La₄(WO₄)₇ is a prerequisite for vibronic operation of Tm lasers above 2 μ m [16].

3.4. Comparison with other Tm³⁺-doped tungstates

In Table 3, we compared absorption and emission properties of Tm³⁺ ions in various representative tungstate crystals, namely tetragonal Tm:Na₂La₄(WO₄)₇ and monoclinic Tm:KLu(WO₄)₂ [9] and Tm:MgWO₄ [10]. Note that it is easier to grow the former crystal (by Czochralski method) as compared to the latter ones (by Top-Seeded-Solution Growth, from the flux). Regarding the ³H₆ → ³H₄ absorption, Tm:Na₂La₄(WO₄)₇ provides almost the same peak σ_{abs} and slightly broader $\Delta\lambda_{\text{abs}}$ (FWHM) as compared to Tm:KLu(WO₄)₂. What about the ³F₄ → ³H₆ emission, Tm:Na₂La₄(WO₄)₇ shows the broader gain bandwidth $\Delta\lambda_{\text{gain}}$. The ³F₄ lifetimes of Tm³⁺ ions are close for the three considered crystals.

4. Laser operation

For the laser experiments, the same 3.1(a)×3.0(c)×3.0(a) mm³ rectangular sample, 1.36 at.% Tm:Na₂La₄(WO₄)₇ was used. It was polished for light propagation along the a and c axes (a -cut and c -cut, respectively). Both pairs of the crystal faces were uncoated. All experiments were performed in the CW mode.

4.1. Hemispherical cavity: a -cut crystal

The CW laser experiments with the a -cut crystal were performed in a hemispherical cavity. The pump mirror (PM) was antireflection (AR) coated at 770-1050 nm and high reflection (HR) coated at 1800-2080 nm. It was placed at 1 mm from the laser crystal. Several concave output couplers (OCs) with radius of curvature R_{OC} of 50 mm and transmission T_{OC} of 1.5%, 3%, 5%, 9% or 15% at the laser wavelength were employed. The total physical cavity length was ~49 mm. The a -cut crystal was mounted in a Cu-holder using Indium foil to provide better thermal contact from all 4 lateral sides. The holder was water-cooled to 12 °C.

The laser crystal was pumped through the PM by a fiber-coupled AlGaAs laser diode (LD) at ~ 802 nm. In contrast to pump at the maximum absorption line at 794 nm, we shifted the pump wavelength to 802 nm reducing the quantum defect to reduce partially the thermal roll-over minimizing the probability of thermal fracture while still providing enough population inversion to overcome the ground state reabsorption therefore realizing efficient laser operation. The fiber details were: core diameter, 200 μm , numerical aperture, N.A. = 0.22. The diode wavelength was stabilized by water-cooling. The unpolarized pump radiation was collimated and focused into the crystal using a lens assembly (focal length: 30 mm, 1:1 reimaging ratio). The pump spot radius in the crystal w_p was 100 μm . The single pass pump absorption of the crystal under lasing conditions amounted to 18%.

The input-output characteristics and the emission spectra of the *a*-cut Tm:Na₂La₄(WO₄)₇ laser are presented in Fig. 7. The π -polarization was naturally selected according to the anisotropy of the gain, Fig. 5. The maximum output power reached 650 mW at ~ 1937 nm corresponding to a slope efficiency η of 31% (with respect to the absorbed pump power P_{abs}), for $T_{\text{OC}} = 1.5\%$. The laser threshold was at $P_{\text{abs}} = 260$ mW. The laser performance deteriorated with the increase of T_{OC} due to up-conversion losses. The laser emission wavelength shifted accordingly from 1937 to 1869 nm which agrees with the gain spectra, Fig. 5(a). The best laser performance in terms of slope efficiency has been obtained with the lowest T_{OC} . This could mean relatively high cavity losses. We attribute this to the Fresnel loss of the two uncoated surfaces of the crystal without placing laser crystal.

Microchip laser concept means a laser material and (optionally) a saturable absorber both placed in a compact plano-plano laser cavity featuring low intracavity losses and potentially high laser efficiency. Tm³⁺-doped tungstate crystals have been recently recognized as very suitable materials for microchip lasers [17]. At first, we studied microchip laser operation with the *a*-cut Tm:Na₂La₄(WO₄)₇ by using a plane OC and approaching both PM and OC to the crystal with minimum air gaps. No laser emission was observed in this case. The reason for this is the negative (defocusing) thermal lens (with the optical power $D < 0$) for the *a*-cut crystal. The physical reason for this phenomenon is the negative thermo-optic coefficient, dn/dT , for all tetragonal double tungstates [8]. However, it is known that solely the negative dn/dT does not presumably lead to $D < 0$. The second key effect is the linear thermal expansion, quantified by the thermal expansion coefficient α which is positive for the majority of the dielectric crystals. The overall variation of the optical path length (OPL) of a laser crystal can be represented by the so-called thermal coefficient of the optical path, $\text{TCOP} = dn_E/dT + (n_E - 1)\alpha_k$. Here, \mathbf{E} and \mathbf{k} vectors indicate the light polarization and light propagation direction, respectively. For an *a*-cut uniaxial crystal and π -polarization, it gives $\text{TCOP}_{a\text{-cut},\pi} = dn_e/dT + (n_e - 1)\alpha_a$. For NaLa(WO₄)₂, this value is $-4.6 \times 10^{-6} \text{ K}^{-1}$ [8] (a negative thermal lens is expected). One can argue that the second available principal light polarization, σ , can be naturally selected in a microchip laser if it provides a positive thermal lens. However, for *a*-cut NaLa(WO₄)₂ and σ -polarization, the above equation changes to $\text{TCOP}_{a\text{-cut},\sigma} = dn_o/dT + (n_o - 1)\alpha_a = -4.0 \times 10^{-6} \text{ K}^{-1}$ [8], meaning a negative thermal lens.

Thus, we approached the concave OC to the *a*-cut crystal to produce a compact laser (total cavity length: ~6 mm). The output performance is presented in Fig. 7(a). This laser generated a maximum output power of 715 mW at ~1937 nm with $\eta = 34\%$ (for $T_{OC} = 1.5\%$).

4.2. Microchip-type cavity: *c*-cut crystal

The analysis of the TCOP can be extended to the *c*-cut crystals, where $TCOP_{c-cut,\sigma} = dn_o/dT + (n_o - 1)\alpha_c$. Although using *c*-cut crystals, for which the laser emission is expected to be unpolarized (randomly polarized), any ray propagating along the *c*-axis (optical axis) will have the σ ($\mathbf{E} \perp \mathbf{c}$) polarization. For $\text{NaLa}(\text{WO}_4)_2$, the $TCOP_{c-cut,\sigma}$ is $+2.7 \times 10^{-6} \text{ K}^{-1}$ (a positive thermal lens is expected). The sharp difference with respect to the *a*-cut crystal is explained mostly by the anisotropy of the thermal expansion, $\alpha_c \gg \alpha_a$, ($\alpha_c/\alpha_a = 1.78$ for $\text{NaLa}(\text{WO}_4)_2$). In this way, the positive contribution of the thermal expansion to the variation of the OPL is dominating over the negative contribution of dn/dT leading to the so-called ‘‘athermal’’ behaviour [8].

This conclusion was verified by testing the *c*-cut $\text{Tm}:\text{Na}_2\text{La}_4(\text{WO}_4)_7$ crystal in a microchip-type laser cavity with all the experimental details being identical to those described in Section 3.1. A set of flat OCs with transmission of 0.1%, 1.5%, 3%, 5% or 9% at the laser wavelength was used. The pump absorption (double-pass, due to the partial reflection of the OC at the pump wavelength) for the *c*-cut crystal was ~27%. Note that the pump absorption efficiency for both the *a*-cut and *c*-cut crystals was limited by the Tm^{3+} concentration. The maximum P_{abs} in this experiment was limited due to the deterioration of the AlGaAs laser diode. The results are shown in Fig. 8. Stable microchip laser operation was achieved. The output laser emission was unpolarized. These findings confirm the positive sign of the thermal lens for the *c*-cut crystal.

The *c*-cut $\text{Tm}:\text{Na}_2\text{La}_4(\text{WO}_4)_7$ laser generated a maximum output power of 340 mW at 1930-1948 nm with $\eta = 41\%$ (for $T_{OC} = 1.5\%$). The laser threshold was at $P_{\text{abs}} = 510 \text{ mW}$. By varying the output coupling from 0.1% to 9%, the emission wavelength experienced a blue-shift of the multi-peak spectrum from 1988-2015 nm to 1883-1887 nm according to the gain spectra, Fig. 5(b).

4.3. Comparison with Tm^{3+} -doped scheelite-type crystals

In Table 4, we compared output characteristics of lasers based on Tm^{3+} -doped scheelite-type crystals, namely tetragonal double tungstates and doubly molybdates, $\text{Tm}:\text{AT}(\text{XO}_4)_2$ (where A = Na or Li, T = Gd, Y, Lu, La, and X = W or Mo), reported so far [1,2,5,18-21]. These crystals were studied under diode- and Ti:Sapphire (Ti:Sa) pumping. Due to the better quality of the pump beam favouring mode-matching, higher slope efficiencies were obtained in the latter case. In Ref. [2], a CW $\text{Tm}:\text{NaLu}(\text{WO}_4)_2$ laser generated 0.50 W at 1924 nm with $\eta = 49\%$. Regarding the diode-pumping, typically, small slope efficiencies were reported even for highly-doped crystals. In Ref. [5], the maximum output power extracted from a CW $\text{Tm}:\text{NaGd}(\text{WO}_4)_2$ laser was 0.33 W at 1997 nm with η of only 8%. Much higher η value of 60% was reported in Ref. [19] whilst for quasi-CW pumping.

The results obtained in the present work represent the highest CW output power achieved from any diode- or Ti:Sa-pumped Tm:AT(XO₄)₂ laser. Moreover, we did not observe the thermal roll-over of the input-output dependence, see Fig. 7(a), which was claimed as a limiting factor for power scaling in [1,5]. The slope efficiency obtained in the present work (34%) is much higher than in the previous reports about diode-pumped CW Tm:AT(XO₄)₂ lasers (~8%) [1,5] despite the relatively low Tm³⁺ doping concentration used in our study.

5. Conclusion

A novel tetragonal scheelite-type double tungstate crystal, Tm:Na₂La₄(WO₄)₇, offers intense and broad polarized spectral bands due to the local disorder (e.g., the gain bandwidth exceeds 100 nm for π -polarization), which is interesting for tunable and ultrashort pulse lasers operating at ~2 μ m. Vibronic laser operation beyond 2 μ m is also expected due to the strong Raman activity. It is known that there are multiple lines of water vapour absorption at 1.8-1.95 μ m which prevent stable mode-locking. However, Tm³⁺-doped crystals can be forced to oscillate at longer wavelength with the aim of spectrally-selective (“bandpass”) cavity mirrors as it has been demonstrated, e.g., with Tm:KLu(WO₄)₂ [22]. Further work will focus on the study of highly Tm³⁺-doped crystals to boost the laser efficiency through the cross-relaxation for Tm³⁺ ions.

Using an *a*-cut Tm:Na₂La₄(WO₄)₇ crystal in a compact diode-pumped laser, we achieved a maximum output power of 715 mW at ~1937 nm with a slope efficiency of 34%. This laser outperforms all known Tm lasers based on the NaT(WO₄)₂ crystals including both pump sources (both with Ti:Sapphire and diode lasers). With a *c*-cut Tm:Na₂La₄(WO₄)₇ crystal, we realized the first CW microchip laser based on a tetragonal tungstate crystals and proved the possibility of “athermal” behavior for this class of tungstates which was theoretically predicted before [8].

Acknowledgements

This work was supported by The National Natural Science Foundation of China (projects No. 61575199, No. 61775217, No. 61705231, No. 11404332, and No. 61475158), Key Project of Science and Technology of Fujian Province (2016H0045), the Strategic Priority Research Program of the Chinese Academy of Sciences (No. XDB20000000); the National Key Research and Development Program of China (No. 2016YFB0701002), the Natural Science Foundation of Fujian Province (No. 2016J01328), the Instrument project of Chinese Academy of Sciences (No. YZ201414), Spanish Government (No. MAT2016-75716-C2-1-R, No. TEC 2014-55948-R), Generalitat de Catalunya (No. 2017SGR755). F.D. acknowledges additional support through the ICREA academia award 2010ICREA-02 for excellence in research. P.L. acknowledges financial support from the Government of the Russian Federation (Grant 074-U01) through ITMO Post-Doctoral Fellowship scheme.

References

1. J. M. Cano-Torres, M. Rico, X. Han, M. D. Serrano, C. Cascales, C. Zaldo, V. Petrov, U. Griebner, X. Mateos, P. Koopmann and C. Kränkel, *Phys. Rev. B* 84 (2011) 174207-1–15.
2. X. Han, J. M. Cano-Torres, M. Rico, C. Cascales, C. Zaldo, X. Mateos, S. Rivier, U. Griebner and V. Petrov, *J. Appl. Phys.* 103 (2008) 083110-1-8.
3. Y. Wei, C. Tu, H. Wang, F. Yang, G. Jia, Z. You, J. Li, Z. Zhu and Y. Wang, *Appl. Phys. B* 86 (2007) 529-535.
4. F. A. Bolschikov, G. M. Kuz'micheva, D. A. Lis, Y. M. Papin, A. V. Popov, P. A. Ryabochkina, V. B. Rybakov, V. G. Senin, V. A. Smirnov, K. A. Subbotin and Y. K. Voron'ko, *J. Cryst. Growth* 311 (2009) 4171-4178.
5. J. M. Cano-Torres, M. D. Serrano, C. Zaldo, M. Rico, X. Mateos, J. Liu, U. Griebner, V. Petrov, F. J. Valle, M. Galán and G. Viera, *J. Opt. Soc. Am. B* 23 (2006) 2494-2502.
6. Y. Yu, Y. Huang, L. Zhang, Z. Lin, S. Sun and G. Wang, *Appl. Phys. B*, 2014, 116, 69-74.
7. V. Morozov, A. Arakcheeva, B. Redkin, V. Sinitsyn, S. Khasanov, E. Kudrenko, M. Raskina, O. Lebedev and G. Van Tendeloo, *Inorg. Chem.* 51 (2014) 5313-5324.
8. P. A. Loiko, X. Han, K. V. Yumashev, N. V. Kuleshov, M. D. Serrano, C. Cascales and C. Zaldo, *Appl. Phys. B* 111 (2013) 279-287.
9. V. Petrov, M. Cinta Pujol, X. Mateos, Ò. Silvestre, S. Rivier, M. Aguiló, R. M. Solé, J. Liu, U. Griebner and F. Díaz, *Laser Photonics Rev.* 1 (2007) 179–212.
10. L. Zhang, H. Lin, G. Zhang, X. Mateos, J. M. Serres, M. Aguiló, F. Díaz, U. Griebner, V. Petrov, Y. Wang, P. Loiko, E. Vilejshikova, K. Yumashev, Z. Lin and W. Chen, *Opt. Express* 25 (2017) 3682-3693.
11. B. R. Judd, *Phys. Rev.* 127 (1962) 750–761.
12. G. S. Ofelt, *J. Chem. Phys.* 37 (1962) 511–520.
13. C. M. Dodson and R. Zia, *Phys. Rev. B* 86 (2012) 125102.
14. A. S. Yasyukevich, V. G. Shcherbitskii, V. E. Kisel', A. V. Mandrik and N. V. Kuleshov, *J. Appl. Spectrosc.* 71 (2004) 202–208.
15. L. Macalik, J. Hanuza and A. A. Kaminskii, *J. Molec. Struct.* 555 (2000) 289-297.
16. P. Loiko, X. Mateos, S. Y. Choi, F. Rotermund, J. M. Serres, M. Aguiló, F. Díaz, K. Yumashev, U. Griebner and V. Petrov, *J. Opt. Soc. Am. B* 33 (2016) D19–D27.
17. J. M. Serres, X. Mateos, P. Loiko, K. Yumashev, N. Kuleshov, V. Petrov, U. Griebner, M. Aguiló and F. Díaz, *Opt. Lett.* 39 (2014) 4247–4250.
18. W. Guo, Y. Chen, Y. Lin, Z. Luo, X. Gong and Y. Huang, *J. Appl. Phys.* 103 (2008) 093106-1-10.
19. Y. J. Chen, Y. F. Lin, W. J. Guo, X. H. Gong, J. H. Huang, Z. D. Luo and Y. D. Huang, *Laser Phys. Lett.* 9 (2012) 141-144.
20. W. Guo, Y. Chen, Y. Lin, X. Gong, Z. Luo and Y. Huang, *J. Phys. D: App. Phys.* 41 (2008) 115409-1-9.
21. J. Tang, Y. Chen, Y. Lin, X. Gong, J. Huang, Z. Luo and Y. Huang, *J. Opt. Soc. Am. B* 27 (2010) 1769-1776.
22. A. Schmidt, S. Y. Choi, D. I. Yeom, F. Rotermund, X. Mateos, M. Segura, F. Diaz, V. Petrov and U. Griebner, *Appl. Phys. Express* 5 (2012) 092704-1-3.

Table 1. Experimental and calculated absorption oscillator strengths for the Tm:Na₂La₄(WO₄)₇ crystal.

Transition	$\langle\lambda\rangle$, nm	$\langle E\rangle$, cm ⁻¹	$\langle I\rangle$, cm ⁻¹ nm	$\langle f_{\text{exp}}^{\text{e}}\rangle$ $\times 10^6$	$\langle f_{\text{calc}}^{\text{e}}\rangle$ $\times 10^6$
³ H ₆ → ³ F ₄	1749	5717	210.81	5.43	5.43 ^{ED}
³ H ₆ → ³ H ₅	1205	8299	59.68	3.24	3.22 ^{ED} +0.52 ^{MD}
³ H ₆ → ³ H ₄	794.6	12585	60.99	7.61	7.34 ^{ED}
³ H ₆ → ³ F ₃	689.8	14495	28.01	4.64	4.20 ^{ED}
³ H ₆ → ¹ G ₄	471.8	21193	7.12	2.52	1.85 ^{ED}
³ H ₆ → ¹ D ₂	360.2	27761	8.03	4.88	-
<i>rms dev.</i>					0.566

$\langle\lambda\rangle$ - “center of gravity” of the absorption band, $\langle E\rangle$ is the corresponding estimated energy of the multiplet barycenter, $\langle I\rangle$ – polarization-averaged integrated absorption coefficient, $\langle f_{\text{exp}}^{\text{e}}\rangle$ – polarization-averaged experimental absorption oscillator strength, $\langle f_{\text{calc}}^{\text{e}}\rangle$ - calculated absorption oscillator strength, ED and MD stand for the electric-dipole and magnetic-dipole contributions, respectively.

Table 2. Calculated emission probabilities for Tm³⁺ in the Na₂La₄(WO₄)₇ crystal.

Excited state	Final state	$\langle\lambda\rangle$, nm	A_{JJ} , s ⁻¹	B_{JJ} , %	A_{tot} , s ⁻¹	τ_{rad} , ms
³ F ₄	³ H ₆	1749	614.8 ^{ED}	100	614.8	1.63
³ H ₅	³ F ₄	3874	21.0 ^{ED} +1.3 ^{MD}	2.9	757.2	1.32
	³ H ₆	1205	635.6 ^{ED} +99.3 ^{MD}	97.1		
³ H ₄	³ H ₅	2333	10.1 ^{ED} +12.3 ^{MD}	0.5	4498	0.22
	³ F ₄	1456	312.7 ^{ED} +27.7 ^{MD}	7.6		
	³ H ₆	794.6	4135 ^{ED}	91.9		
³ F ₃ + ³ F ₂	³ H ₄	5233	8.5 ^{ED} +0.3 ^{MD}	0.2	5127	0.195
	³ H ₅	1614	1075 ^{ED}	20.9		
	³ F ₄	1139	214.3 ^{ED} +68.4 ^{MD}	5.5		
	³ H ₆	689.9	3759 ^{ED}	73.3		
¹ G ₄	³ F ₂	1610	21.3 ^{ED}	0.3	6970	0.143
	³ F ₃	1493	121.8 ^{ED} +4.1 ^{MD}	1.8		
	³ H ₄	1162	831.2 ^{ED} +40.1 ^{MD}	12.5		
	³ H ₅	775.6	2256 ^{ED} +184.2 ^{MD}	35.0		
	³ F ₄	646.2	406.3 ^{ED} +11.2 ^{MD}	5.9		
	³ H ₆	471.9	3095 ^{ED}	44.4		

$\langle\lambda\rangle$ - mean wavelength of the emission band, A_{JJ} – probability of radiative spontaneous transition, B_{JJ} – luminescence branching ratio, A_{tot} – total probability of radiative spontaneous transitions from the excited-state, τ_{rad} – its radiative lifetime. ED and MD stand for the electric-dipole and magnetic-dipole contributions, respectively.

Table 3. Comparison of spectroscopic properties of Tm³⁺ ions in various tungstate crystals.

No.	λ_{abs} , nm	σ_{abs} , 10 ⁻²⁰ cm ²	$\Delta\lambda_{\text{abs}}$, nm	λ_{em} , nm	σ_{SE} , 10 ⁻²⁰ cm ²	$\Delta\lambda_{\text{gain}}$, nm	τ_{Tm} , ms
1	794.5	4.86(σ)	5.3(σ)	1940	0.36(π)	110(π)	1.63
2	801.9	5.1(m)	4.1(m)	1946	1.3(m)	84(m)	1.34
3	802.6	2.04(x)	14(x)	2020	0.82(y)	82(y)	1.95

No.1 – Tm:Na₂La₄(WO₄)₇ (this work), No.2 – Tm:KLu(WO₄)₂ (Ref. [9]), No.3 – Tm:MgWO₄ (Ref. [10]). The light polarization is indicated in brackets.

Table 4. Output characteristics of lasers based on Tm³⁺-doped tetragonal scheelite-type tungstates reported so far.

Crystal	Doping	Pump	P_{out} , W	λ_{L} , nm	η , %	Ref.
Tm:Na ₂ La ₄ (WO ₄) ₇	1.36 at.%	diode	0.72	1937	34	*
Tm:NaGd(WO ₄) ₂	3.7 at.%	diode	0.33	1997	8	[5]
Tm:NaY(WO ₄) ₂	5 at.%	diode	0.21	1930	7.5	[1]
Tm:NaLa(MoO ₄) ₂	7.5 at.%	diode**	0.14	1886	60	[19]
Tm:NaLu(WO ₄) ₂	5.9 mol%	Ti:Sa	0.50	1924	49	[2]
Tm:NaY(WO ₄) ₂	7.9 at.%	Ti:Sa	0.40	1923	43	[1]
Tm:NaLa(MoO ₄) ₂	7.5 at.%	Ti:Sa	0.50	1900	50	[18]
Tm:NaGd(MoO ₄) ₂	4.6 at.%	Ti:Sa**	0.17	1905	25	[20]
Tm:LiGd(MoO ₄) ₂	5.4 at.%	Ti:Sa**	0.29	1900	28	[21]

*This work. **Quasi-CW operation.

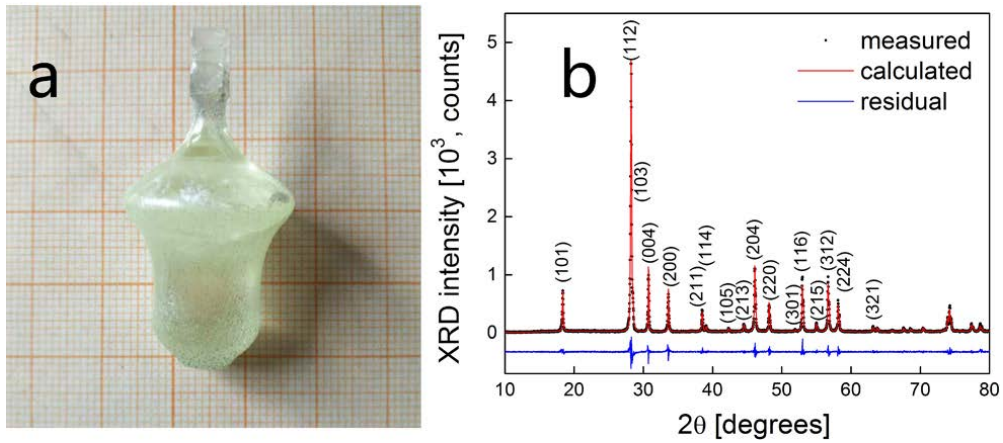


Figure 1. (a) Photograph of the as-grown $\text{Tm}:\text{Na}_2\text{La}_4(\text{WO}_4)_7$ boule; (b) Rietveld analysis of the XRD pattern of this crystal. Numbers denote the Miller's indices, (hkl) .

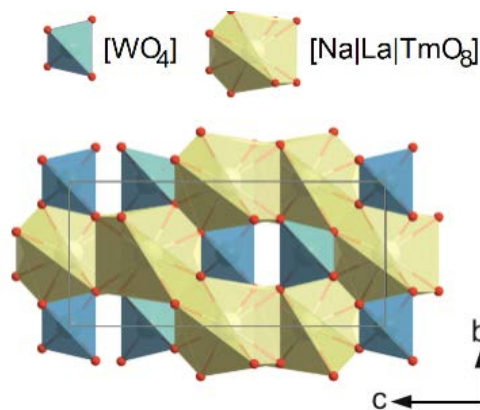


Figure 2. Fragment of structure of $\text{Tm}:\text{Na}_2\text{La}_4(\text{WO}_4)_7$ in projection to the b - c plane. *Grey rectangle* – unit-cell.

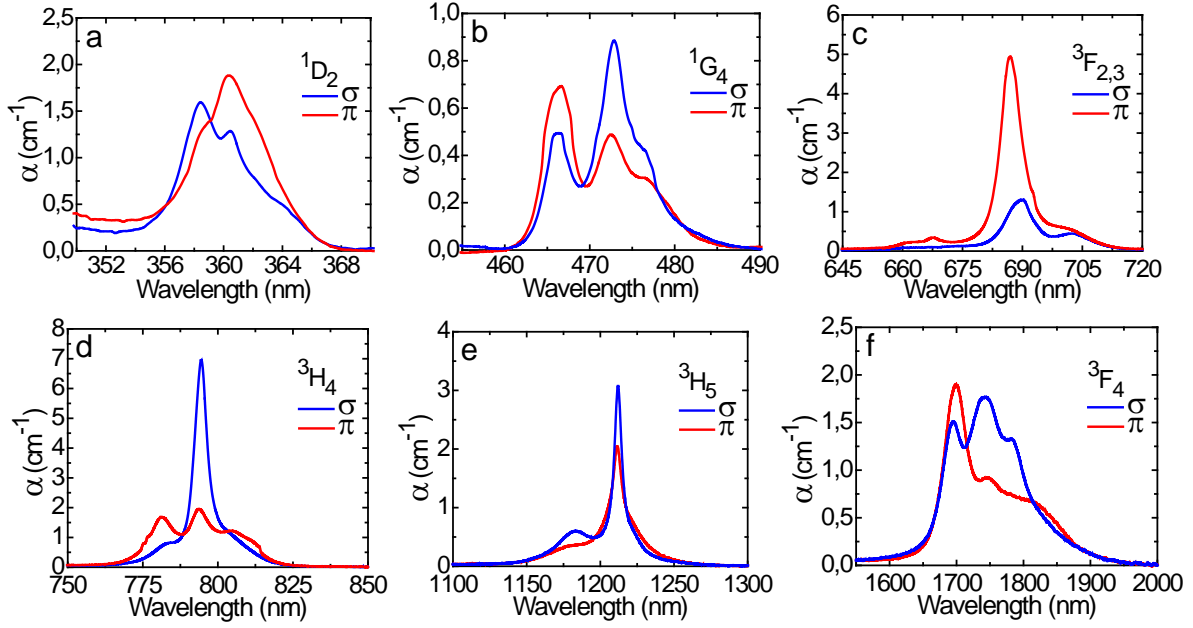


Figure 3. (a-f) Absorption spectra of a 1.36 at.% Tm:Na₂La₄(WO₄)₇ crystal, light polarization is $\mathbf{E} \parallel \mathbf{c}$ (π) and $\mathbf{E} \perp \mathbf{c}$ (σ).

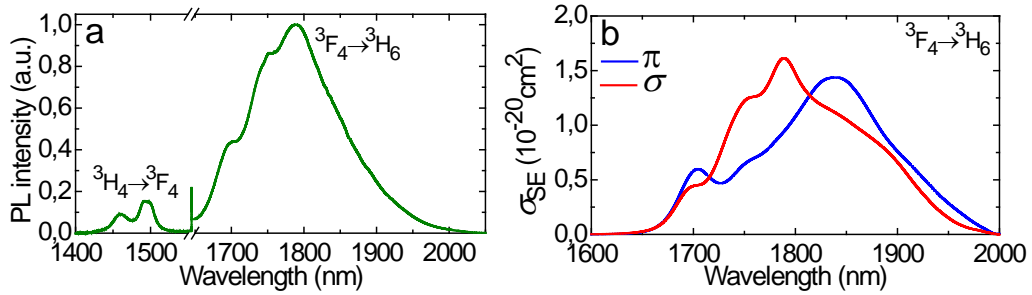


Figure 4. Emission properties of the Tm:Na₂La₄(WO₄)₇ crystal: (a) unpolarized luminescence spectrum, $\lambda_{\text{exc}} = 802$ nm (excitation to the $^3\text{H}_4$ state); (b) stimulated-emission cross-section, σ_{SE} , for the $^3\text{F}_4 \rightarrow ^3\text{H}_6$ transition of Tm^{3+} calculated by the modified reciprocity method, light polarization is $\mathbf{E} \parallel \mathbf{c}$ (π) and $\mathbf{E} \perp \mathbf{c}$ (σ); (c) luminescence decay curve: *symbols* – experimental data, *line* – single-exponential fit, $\lambda_{\text{exc}} = 802$ nm, $\lambda_{\text{lum}} = 1800$ nm.

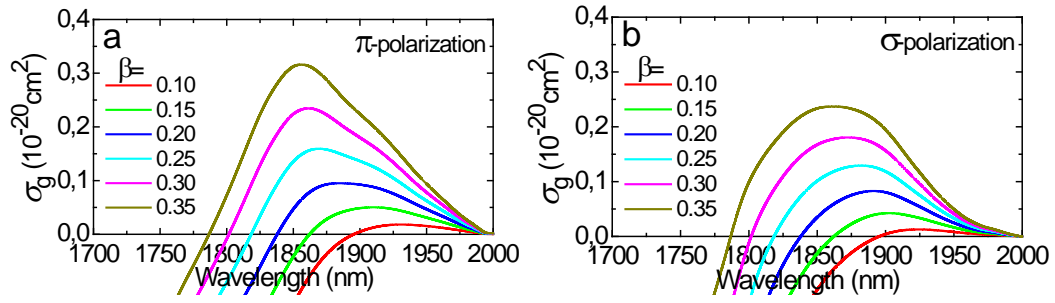


Figure 5. Gain cross-section, $\sigma_g = \beta\sigma_{SE} - (1-\beta)\sigma_{abs}$, for the ${}^3F_4 \rightarrow {}^3H_6$ transition of Tm^{3+} in $Na_2La_4(WO_4)_7$ for light polarization (a) $\mathbf{E} \parallel \mathbf{c}$ (π) and (b) $\mathbf{E} \perp \mathbf{c}$ (σ), β : inversion ratio.

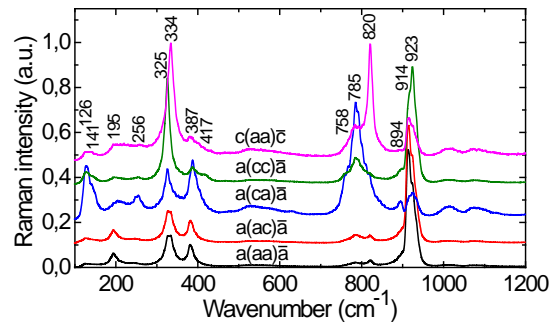


Figure 6. Polarized Raman spectra of a -cut and c -cut $Tm:Na_2La_4(WO_4)_7$ crystals. The excitation wavelength is 514 nm.

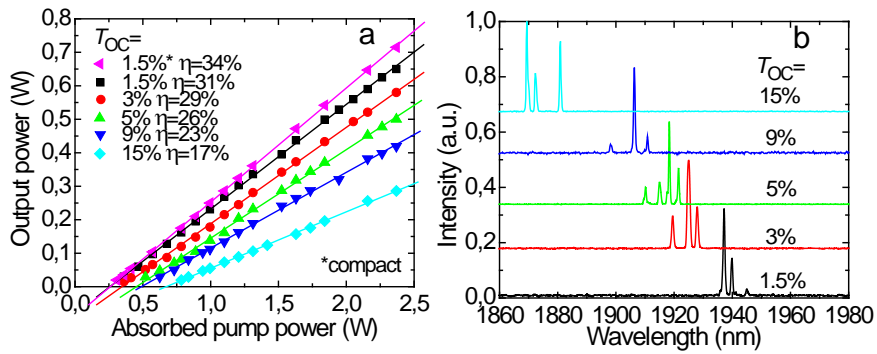


Figure 7. CW $Tm:Na_2La_4(WO_4)_7$ laser in a hemispherical cavity (compact plane-concave cavity) - a -cut crystal: (a) input-output dependences, η – slope efficiency; (b) typical laser emission spectra measured at $P_{abs} = 2.4$ W. The laser polarization is π .

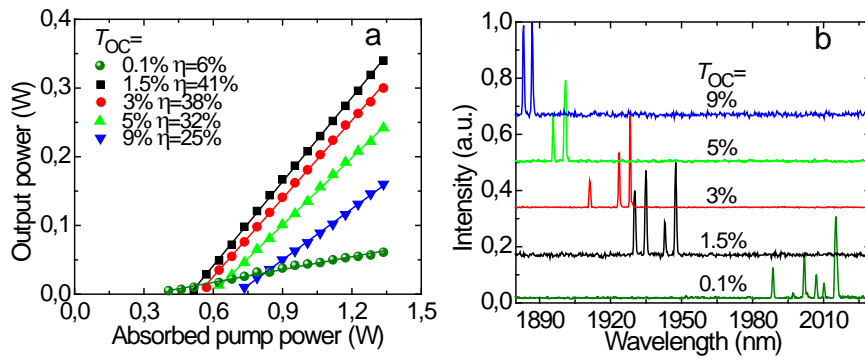


Figure 8. CW Tm:Na₂La₄(WO₄)₇ laser in a microchip-type cavity - *c*-cut crystal: (a) input-output dependences, η – slope efficiency; (b) typical laser emission spectra measured at $P_{\text{abs}} = 1.33$ W. The laser output is unpolarized.